

ON THE 70th ANNIVERSARY OF THE INSTITUTE OF RADIOENGINEERING
AND ELECTRONICS, RUSSIAN ACADEMY OF SCIENCES

Study of Superconducting Transmission Lines and Tunnel Junctions for Signal Detection at Frequencies above 1 THz

N. V. Kinev^{a, *}, A. M. Chekushkin^a, F. V. Khan^a, and K. I. Rudakov^b

^a Kotelnikov Institute of Radioengineering and Electronics, Russian Academy of Sciences, Moscow, 125009 Russia

^b Editorial Board of the Journal “Radiotekhnika i Elektronika”, Moscow, 125009 Russia

*e-mail: nickolay@hitech.cplire.ru

Received April 28, 2023; revised April 28, 2023; accepted May 25, 2023

Abstract—Superconducting integrated circuits based on NbTiN/Al transmission lines at frequencies of up to 1.1 THz have been developed and experimentally investigated. The numerical simulation has been carried out for two topologies of a microcircuit with an operating frequency range of 0.9–1.2 THz, which contains a slot antenna formed in the NbTiN thin film and output-matched with a microstrip transmission line and a superconductor–insulator–superconductor (SIS) tunnel junction with an area of $\sim 1 \mu\text{m}^2$ acting as a terahertz detector. Experimental samples of the microcircuit have been fabricated and tested in an experimental setup utilizing a backward-wave oscillator with an output frequency of up to 1.1 THz used as a source. The powerful pumping of the SIS detector has been obtained to demonstrate the applicability of the fabricated NbTiN/Al transmission lines for operation in superconducting circuits at frequencies above 750 GHz, where the conventional Nb/Nb transmission lines cannot operate due to high losses.

DOI: 10.1134/S1064226923090127

INTRODUCTION

Currently, receivers of terahertz range are used in many fields, including study of the atmosphere and space, communication technology, biomedicine, and fundamental materials science and molecular spectroscopy research [1–3]. At this time, the most sensitive THz detectors are superconductor–insulator–superconductor (SIS) junctions due to the low temperature and strong nonlinearity of their characteristics caused by tunneling of quasiparticles through a barrier layer [4]. In most of the available tunnel junction-based receiving systems, niobium (e.g., Nb/AlO_x/Nb) or niobium nitride (e.g., Nb/AlN/NbN) SIS junction electrodes operating at a liquid helium boiling point (4.2 K) are used. Some modern problems related mainly to quantum computations are solved using the aluminum-based SIS junctions [5], but to operate, they require ultralow (about 300 mK and lower) temperatures and, consequently, technically complex cooling systems. In niobium-based junctions, the conventional signal transmission lines are niobium thin films fabricated in the single magnetron sputtering cycle with tunnel junction electrodes. Such transmission lines have a maximum operating frequency of ~ 750 GHz, above which the loss in films increase significantly, according to the Mattis–Bardeen theory [6]. This fundamental limitation is dictated by energy gap Δ of superconducting materials. Thus, in the systems operating at frequen-

cies of up to 1 THz and higher, higher-frequency transmission lines made of materials with a higher Δ value must be used. The most suitable for operation at such frequencies are the NbTiN transmission lines with a fundamental limitation of ~ 1.4 THz [7, 8].

Objective—To develop, fabricate, and test superconducting integrated circuits for studying the characteristics of the NbTiN/Al transmission lines with operating frequencies of up to 1.1 THz.

1. DEVELOPMENT AND FABRICATION OF EXPERIMENTAL MICROCIRCUIT SAMPLES

1.1. Basic Design and Numerical Model of the Integrated Circuits

Two different integrated circuit topologies were developed and numerically simulated, which contain the Nb/AlN/NbN SIS junctions included in a THz transmission line with a NbTiN bottom electrode and an Al top electrode (hereinafter referred to as NbTiN/Al) and acting as detectors of external THz signals. Topology no. 1 of a THz microstrip line (THz-MSL) microcircuit and topology no. 2 of a microcircuit representing a terahertz microstrip line with a resonator (THz-MSLR) are shown in Figs. 1a and 1b, respectively. Both topologies consist of an input slot antenna formed in the lower electrode of the NbTiN integrated structure, detectors based on dou-

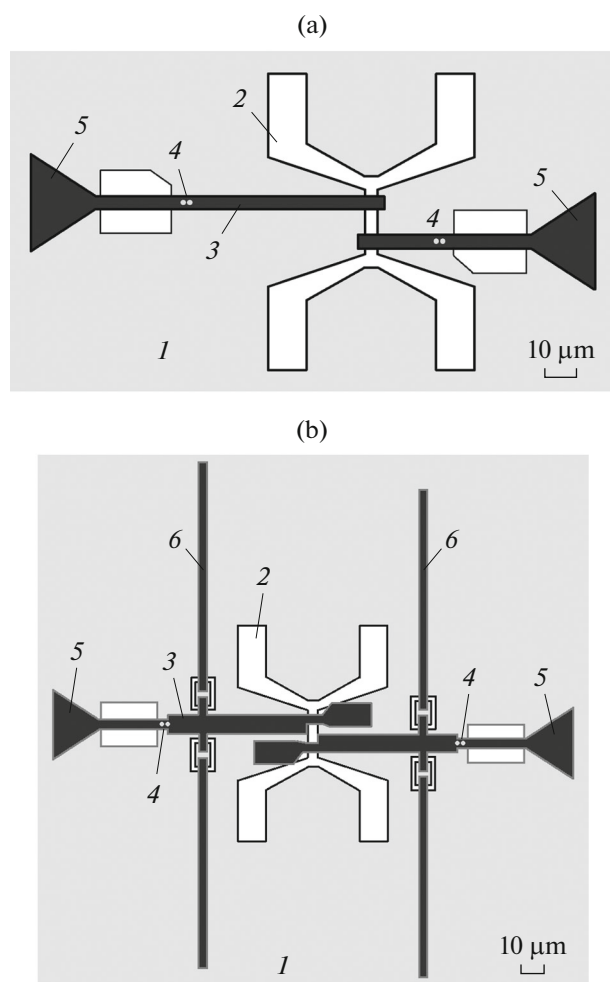


Fig. 1. Topology of the THz integrated structures (a) THz-MSL and (b) THz-MSLR: (1) bottom electrode of the NbTiN-based structure, (2) slot antenna, (3) top electrode of the Al-based structure, (4) Nb/AlN/NbN-based double SIS junction with an area of $1 \mu\text{m}^2$ each, (5) microwave stub, and (6) resonator.

ble SIS junctions connected in parallel with an area of $1 \mu\text{m}^2$ each, and the investigated transmission line input-matched with the antenna and output-matched with the SIS junctions. Double SIS junctions are used instead of single ones in order to broaden the receiving bandwidth via mutual detuning of the capacitance of the junctions by the inductance connecting their lines. In the THz-MSL topology, conventional microstrip line segments with lengths $\lambda/4$ (hereinafter referred to as the short section) and $3\lambda/4$ (hereinafter referred to as the long section) are used (λ is the received radiation wavelength). Below, the difference between the power received by the detector in the long and short sections will allow us to evaluate losses in the microstrip line and determine the parameters of the thin films. In the THz-MSLR topology, two symmetrical segments of a microstrip line with a built-in resonator, which are identical in geometrical dimensions,

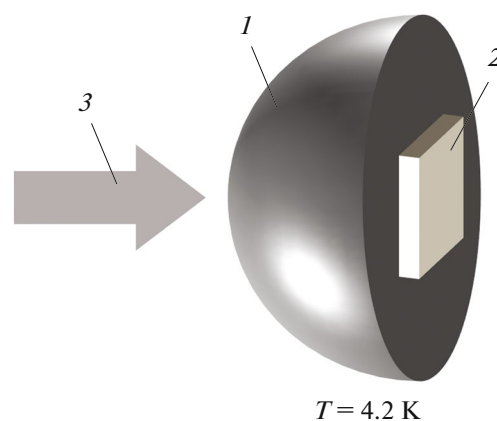


Fig. 2. Scheme of the setup with semi-elliptical silicon lens (1) of microcircuit (2) with investigated structure for detection of the THz radiation (3).

are used; later on, this will make it possible to evaluate losses in the line from the resonator Q factor. The antennas in the two topologies of the integrated structure are designed identically. The microcircuit is mounted at the focus of a semi-elliptical silicon lens, which forms a quasi-optical lens–antenna receiving path (see Fig. 2). A cryogenic module with the integrated structure is placed in a vacuum filling cryostat with an operating temperature of 4.2 K.

The numerical simulation of the microcircuit topologies was carried out in the Ansys HFSS 3D electromagnetic simulation software, which allows simulation of complex structures taking into account the edge effects, boundary conditions, and mutual interference of circuit elements. Since the program does not have a built-in technique for taking into account the properties of superconducting materials, the method proposed in [9, 10] was used. At the first stage, a data array for the surface impedance of superconducting films is formed using the Mattis–Bardn theory relations [6]. Specific parameters of the NbTiN films were borrowed from [11], in which the results were obtained using time-resolved spectroscopy and the investigated thin-film samples were fabricated using the same technology as in this study. At the second stage, the obtained data array is introduced into the Ansys HFSS numerical program and the boundary conditions on the surface of superconducting electrodes are set.

In the numerical model, SIS junction impedance Z_{SIS} is determined by normal-state junction resistance R_{norm} and its capacity C connected in parallel, which can be specified in the program by a special concentrated RLC element (hereinafter referred to as RLC). The SIS junctions were specified as the series-connected RLC and lumped port with a resistance of $R_p = 1 \text{ m}\Omega$, much lower than R_{norm} . Since each section of the integrated circuit contains two SIS junctions dis-

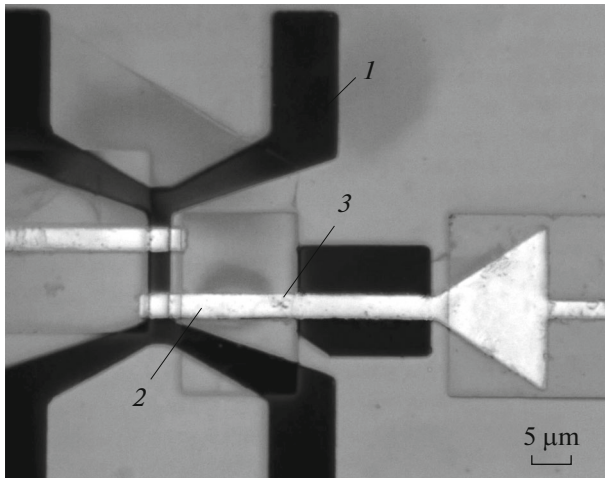


Fig. 3. Microphotograph of the central part of the THz-MSL-topology microcircuit (short section): (1) slot antenna, (2) microstrip transmission line, and (3) double SIS junction with an area of $1 \mu\text{m}^2$ each.

tant by $2 \mu\text{m}$, the junctions are taken into account in the model as two independent objects. To calculate detected power P_{det} (dB), which is equivalent in the numerical model to the power absorbed by the double SIS junction in each section, formula

$$P_{\text{det}} = 10 \log \left[|S_{21}^{p1}|^2 \left(\text{Re}(Z_{\text{SIS}})/R_p \right) + |S_{21}^{p2}|^2 \left(\text{Re}(Z_{\text{SIS}})/R_p \right) \right], \quad (1)$$

was used, where S_{21}^{p1} and S_{21}^{p2} are the S parameters calculated on the two ports corresponding to each SIS junction in the section.

1.2. Fabrication of the Experimental Samples

The experimental samples of the thin-film microcircuits were fabricated by magnetron sputtering and UV optical lithography; photomasks were formed by electron beam lithography at the submicron size accuracy. The technology for manufacturing the Nb/AlN/Nb and Nb/AlN/NbN tunnel junctions using conventional Nb/Nb transmission lines was described in detail in [12, 13] and the technology of tunnel junctions built into the NbTiN/Al transmission lines was discussed in [14, 15]. All the structures were formed on a high-resistance ($>5 \text{ k}\Omega \text{ cm}$) polished silicon substrate. A 100-nm-thick Al_2O_3 buffer layer was deposited onto the substrate and a 325-nm-thick NbTiN film was deposited on top of it over the entire substrate surface. Then, the film was etched via a resistive mask by plasma chemical etching in the CF_4 medium to form the lower electrode of the transmission line. At the next stage, an Nb/Al–AlN/NbN (80 nm/6 nm–1 nm/80 nm) SIS tunneling structure was formed and etched via a resistive mask to the

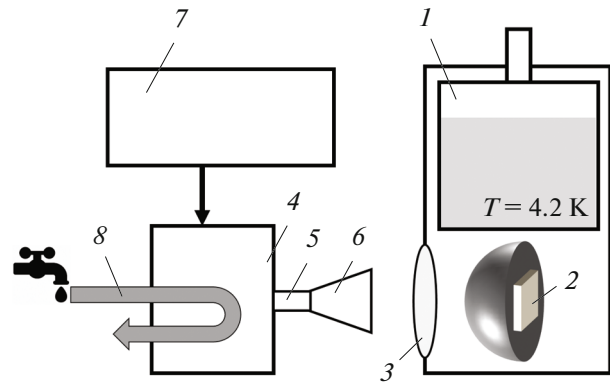


Fig. 4. Scheme of the experimental setup for studying the superconducting integrated structures: (1) filling cryostat, (2) microcircuit with the investigated structure, (3) cryostat input window, (4) BWO, (5) BWO output waveguide, (6) BWO output horn, (7) BWO power supply, and (8) BWO water cooling system.

NbTiN layer. At this stage, the surface of the lower NbTiN electrode layer and the ends of the SIS junctions were anodized; after that, the 400-nm-thick SiO_2 insulating layer was deposited. These procedures ensured high-quality insulation between the lower and upper electrodes. At the final stage, the top Al-based electrode with a thickness of 500 nm was deposited. A microphotograph of the fabricated structure (a fragment of the long section of the THz-MSL topology) is presented in Fig. 3.

1.3. Experimental Setup

The structures were cooled using a vacuum cryostat (4.2 K) filled with liquid helium. To pump the SIS detectors with a THz signal and study the properties of the transmission lines, a high-power source based on a backward-wave oscillator (BWO) with the operating frequency range of about 0.9–1.1 THz was used as an external oscillator. The BWO is a water-cooled oscillator controlled by cathode voltage V_c of a delay line system in the range of 4–6 kV. To ensure a sufficiently narrow output radiation beam, an additional horn antenna is installed at the BWO waveguide output. A cryostat entrance window is made of Mylar, which is almost transparent in the THz frequency range. A scheme of the experimental setup is shown in Fig. 4. Since the patterns of both the BWO output signal and the receiving signal of the antenna–lens system are quite narrow, the fine optical alignment of the mutual positions of the BWO and the cryostat (more than 20 kg each) was a rather difficult task. In addition, the measuring system is highly sensitive to minor mechanical vibrations and position deviations; therefore, the experimental stand was placed on a massive table.

2. EXPERIMENTAL RESULTS AND DISCUSSION

The effect of the THz signal of the BWO on the detector was fixed by measuring the I – V characteristics of the SIS junction. For accurate I – V measurements, a low-noise battery-powered set and measurement unit was specially designed. The I – V characteristics of the SIS junctions were measured in the voltage (up to 7 mV) setting mode. In this case, the characteristic currents through the junction were approximately 0.8–1 mA. The families of the measured I – V characteristics of the SIS junctions for the short and long sections of the THz-MSL topology and for one of the identical sections of the THz-MSLR topology are shown in Fig. 5. Normal resistances R_{norm} of the junction for the presented characteristics are 7.14 Ω (Fig. 5a), 6.86 Ω (Fig. 5b), and 6.52 Ω (Fig. 5c). The highest detected power level corresponds to the uppermost curves in Figs. 5a–5c. The BWO-based source used has an output frequency of 1.035 THz at $V_c = 5$ kV and a linear frequency tuning factor of ~ 70.73 GHz/kV. The pumping of the SIS detectors of the experimental samples of both topologies was observed in the range of 1.02–1.1 THz. It should be noted that, according to the manufacturer's specification, the BWO used also operates at lower frequencies (up to 0.94 THz); however, in the experiment, the power at frequencies below 1.02 THz turned out to be insufficient to visually change the I – V characteristic of the SIS junction.

The impact of a THz signal on the SIS junction leads simultaneously to two independent effects of a stepwise increase in the tunneling current: the appearance of Shapiro steps [16] and quasiparticle steps [4]. Since the critical current of the junction is not suppressed, a pronounced first Shapiro step appears in the I – V characteristics of the SIS junctions at voltages of 2.12–2.25 mV, which corresponds to a pump frequency of 1.025–1.088 THz from the Josephson constant $2e/h = 483.6$ GHz/mV (e is the elementary charge and h is the Planck's constant), as well as a weak second Shapiro step at a voltage of ~ 4.4 mV corresponding to the doubled frequency. One can see the exact correspondence between the relative positions of the first stage in the I – V characteristic and the pump frequency: the higher the pump frequency, the higher the voltage of the step. It is interesting to note the extremely efficient signal detection in the short section of the THz-MSL topology at which pumping saturated (curve 7 in Fig. 5a).

The numerically calculated detected powers for the THz-MSL topology in the short and long sections are presented in Fig. 6a. The frequencies of the most efficient detection for two sections almost (accurate to 10 GHz) coincide: ~ 0.93 THz. At the same time, the detected power in the long section in the vicinity of 1.05 THz is almost an order of magnitude (8 dB) lower than in the short section, as shown in Fig. 6a by curve 3,

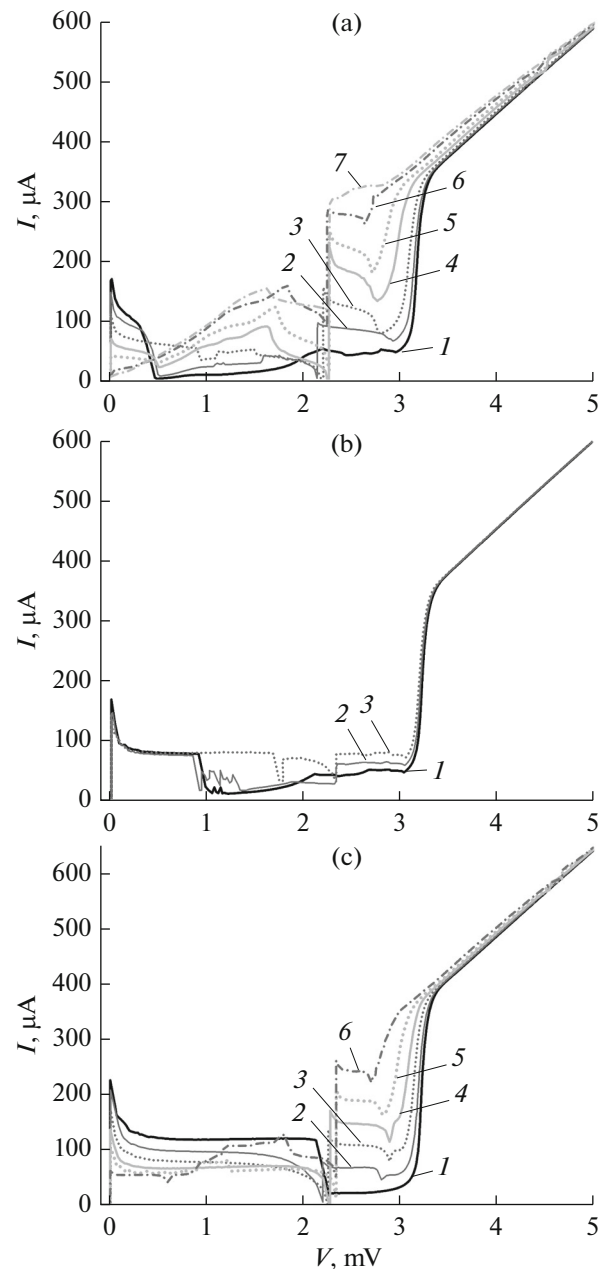


Fig. 5. Series of I – V characteristics of the SIS junction (a) in the short and (b) long section of the THz-MSL topology and (c) in the receiving section of the THz-MSLR topology (I) without external influence and under the influence of BWO signals of different powers and frequencies: (a) 1.032 (2), 1.060 (3), 1.088 (4), 1.09 (5), 1.079 (6), and 1.092 THz (7); (b) 1.102 (2) and 1.103 THz (3); and (c) 1.1038 (2), 1.1064 (3), 1.1074 (4), 1.1104 (5), and 1.1105 THz (6).

which is the difference between the detected power in the short and long sections.

Thus, the results of the calculation correspond to the experimental ones, in which the pumping in the long section turned out to be much lower than in the short one (compare Figs. 5a and 5b). The numerical

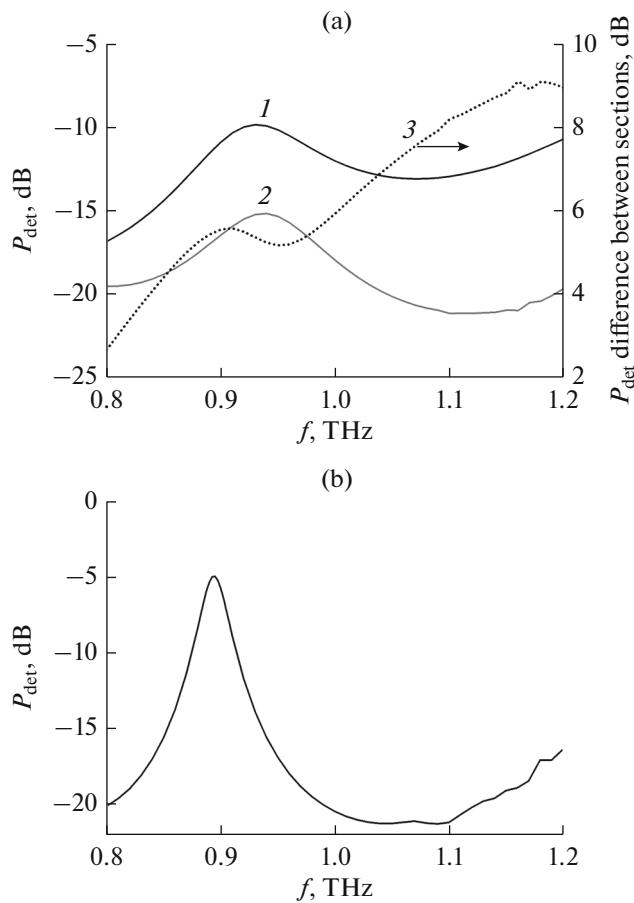


Fig. 6. Results of the numerical calculation of the detected power for (a) the THz-MSL topology in (1) the short and (2) long sections and (3) difference between them and (b) for the THz-MSLR topology.

data on the detected power for the two identical sections of the THz-MSLR topology are presented in Fig. 6b. The effective pumping peak being significantly narrower in frequency in the numerical calculation as compared with the THz-MSL topology is caused by the presence of a resonator, the Q factor of which allows one to evaluate later the characteristics of thin films of the transmission lines. For this topology, a sufficiently powerful pumping of the SIS detector was also experimentally obtained (curve 6 in Fig. 5c), which, however, does not lead to saturation.

Importantly, both developed topologies make it possible to evaluate the characteristics of absorption in the transmission line: from the frequency dependence of the difference between the detected powers in the long and short sections in the investigated range in the THz-MSL topology and from the frequency dependence of the detected power under the condition of either the output power characteristic uniform in frequency or the strictly known dependence of the output power on the absolute value of frequency in the THz-MSLR topology. The power of the BWO output signal

is strongly nonuniform in frequency, unknown in the absolute value, and can be significantly different for two closely spaced frequencies; therefore, such a source does not meet the requirements for setting up a good-quality experiment on estimating the parameters of attenuation in the films. Thus, to carry out such an experiment in the future, it is sufficient to have a radiation source that is weaker in power than a BWO, but uniform in frequency in the range of 0.9–1.1 THz.

CONCLUSIONS

The integrated structures based on SIS junctions are highly sensitive receiving systems capable of operating at frequencies of up to 1 THz and higher; however, the fabrication of transmission lines and the optimization of their design for specific tasks are rather difficult. In this study, two topologies of integrated structures based on the Nb/AlN/NbN SIS junctions with a receiving antenna built into the NbTiN/Al transmission lines with an operating frequency range of 0.9–1.2 THz were developed, numerically simulated, fabricated, and experimentally investigated. A BWO was used as an external THz radiation source and a quasi-optical antenna–lens system was used as a feeder. A powerful pumping of the SIS detectors in the range of 1.02–1.1 THz was obtained, which demonstrated the successful operation of the developed SIS junctions and transmission lines for tasks with target frequencies above 1 THz.

ACKNOWLEDGMENTS

The authors thank A.M. Baryshev for help with numerical calculations. The authors are grateful for the opportunity to access Unique Scientific Unit (USU) no. 352529 Cryointegral, which was used to fabricate the samples and carry out the investigations.

FUNDING

The development of the technology, fabrication of the samples, and the experiment were supported by the Russian Science Foundation, project no. 23-79-00019, <https://rscf.ru/project/23-79-00019/>; the numerical calculation was carried out within the framework of the state task at the Kotelnikov Institute of Radioengineering and Electronics, Russian Academy of Sciences; and operation of the Unique Scientific Unit, project no. 352529 “Cryointegral” was supported by the Ministry of Science and Higher Education of the Russian Federation, agreement no. 075-15-2021-667.

CONFLICT OF INTEREST

The authors declare that they have no conflicts of interest.

REFERENCES

1. S. L. Dexheimer, *Terahertz Spectroscopy: Principles and Applications* (CRC Press, New York, 2008).
<https://doi.org/10.1201/9781420007701>
2. D. F. Plusquellic, K. Siegrist, E. J. Heilweil, and O. Esenturk, *ChemPhysChem* **8** (17), 2412 (2007).
<https://doi.org/10.1002/cphc.200700332>
3. A. G. Davies, A. D. Burnett, W. Fan, et al., *Mater. Today* **11** (3), 18 (2008).
[https://doi.org/10.1016/S1369-7021\(08\)70016-6](https://doi.org/10.1016/S1369-7021(08)70016-6)
4. J. R. Tucker and M. J. Feldman, *Rev. Mod. Phys.* **57**, 1055 (1985).
<https://doi.org/10.1103/RevModPhys.57.1055>
5. A. Vettoliere, R. Satariano, R. Ferraiuolo, et al., *Nanomaterials* **12** (23), 4155 (2022).
<https://doi.org/10.3390/nano12234155>
6. D. C. Mattis and J. Bardeen, *Phys. Rev.* **111** (2), 412 (1958).
<https://doi.org/10.1103/PhysRev.111.412>
7. J. W. Kooi, J. A. Stern, G. Chattopadhyay, et al., *Int. J. Infrared and Millimeter Waves* **19** (3), 373 (1998).
<https://doi.org/10.1023/A:1022595223782>
8. B. D. Jackson, et al., *IEEE Trans. Appl. Supercond.* **11**, 653 (2001).
<https://doi.org/10.1109/77.919429>
9. A. R. Kerr and S. K. Pan, *Intern. J. Infrared and Millimeter Waves* **11** (10), 1169 (1990).
<https://doi.org/10.1007/BF01014738>
10. V. Belitsky, C. Risacher, M. Pantaleev, and V. Vassilev, *Intern. J. Infrared and Millimeter Waves* **27** (1), 809 (2006).
<https://doi.org/10.1007/s10762-006-9116-5>
11. A. Khudchenko, B. N. R. Lap, K. I. Rudakov, et al., *IEEE Trans. Appl. Supercond.* **32** (4), 1500506 (2022).
<https://doi.org/10.1109/TASC.2022.3147736>
12. P. N. Dmitriev, I. L. Lapitskaya, L. V. Filippenko, et al., *IEEE Trans. Appl. Supercond.* **13** (2), 107 (2003).
<https://doi.org/10.1109/TASC.2003.813657>
13. A. Khudchenko, A. M. Baryshev, K. I. Rudakov, et al., *IEEE Trans. on Terahertz Sci. & Technol.* **6** (1), 127 (2016).
<https://doi.org/10.1109/TTHZ.2015.2504783>
14. M. Yu. Fominsky, L. V. Filippenko, A. M. Chekushkin, et al., *Electronics* **10** (23), 2944 (2021).
<https://doi.org/10.3390/electronics10232944>
15. A. M. Chekushkin, L. V. Filippenko, M. Yu. Fominskii, and V.P. Koshelets, *FTT* **64**, 1399 (2022).
16. C. C. Grimes and S. Shapiro, *Phys. Rev.* **169**, 397 (1968).
<https://doi.org/10.1103/PhysRev.169.397>

Translated by E. Bondareva